

The energy landscape of silicon systems and its description by force fields, tight binding schemes, density functional methods and Quantum Monte Carlo methods

S. Alireza Ghasemi¹, Maximilian Amsler¹, Richard G. Hennig²,
Shantanu Roy¹, Stefan Goedecker^{1,*}, C. J. Umrigar³, Luigi
Genovese⁴, Thomas J. Lenosky⁵, Tetsuya Morishita⁶, Kengo Nishio⁶

¹ *Department of Physics, Universität Basel,
Klingelbergstr. 82, 4056 Basel, Switzerland*

² *Department of Materials Science and Engineering,
Cornell University, Ithaca, NY 14850, USA*

³ *Laboratory of Atomic and Solid State Physics,
Cornell University, Ithaca, New York 14853, USA*

⁴ *European Synchrotron Radiation Facility,
6 rue Horowitz, 38043 Grenoble (France)*

⁵ *C8 Medisensors, Los Gatos, CA 95032 and*

⁶ *Research Institute for Computational Sciences (RICS),
National Institute of Advanced Industrial Science and Technology (AIST),
1-1-1 Umezono, Tsukuba, Ibaraki 305-8568, Japan **

(Dated: February 13, 2022)

Abstract

The accuracy of the energy landscape of silicon systems obtained from various density functional methods, a tight binding scheme and force fields is studied. Quantum Monte Carlo results serve as quasi exact reference values. In addition to the well known accuracy of DFT methods for geometric ground states and metastable configurations we find that DFT methods give a similar accuracy for transition states and thus a good overall description of the energy landscape. On the other hand, force fields give a very poor description of the landscape that are in most cases too rugged and contain many fake local minima and saddle points or ones that have the wrong height.

I. INTRODUCTION

In spite of the great progress in density functional methods for treating large systems, it is at present not possible to treat systems with more than about 1000 atoms in complex simulations where forces and energies have to be evaluated many times. This is for instance necessary in molecular dynamics simulations where one has to follow the evolution of the system over long time intervals or in global optimization methods for finding the ground state geometry. In these kinds of situations faster and more approximate methods such as force fields or tight binding schemes are widely used. Because of its technological importance several widely used force fields exist for silicon and large scale simulations, which are not feasible with density functional methods, are frequently performed using these more approximate methods.

These force fields are typically fitted to a data set of ground state structures, usually containing crystalline structures and sometimes also non-periodic structures. An accurate description of some ground state geometries is however not sufficient to ensure accurate dynamical simulations. Dynamical properties such as diffusion coefficients are related to other properties of the energy landscape such as barrier heights. The distribution of barrier heights and other properties of the silicon potential energy surface (PES) have been studied using forcefields¹. In this paper we study overall properties of the energy landscape which are relevant in many different contexts. We look in particular at the accuracy of the barrier heights in the various schemes used for large scale simulations of silicon systems. Since it is known that the barrier heights relevant to chemical reactions are not very well described with standard density functionals such as local density approximation (LDA)² or Perdew-Burke-Ernzerhof (PBE),³ we benchmark some of the energy barriers using accurate quantum Monte Carlo methods. There are two forms of QMC methods that are used for electronic structure calculations, the simpler variational Monte Carlo (VMC) and the more sophisticated diffusion Monte Carlo (DMC). In VMC, quantum mechanical expectation values are calculated using Monte Carlo techniques to evaluate the many-dimensional integrals. The accuracy of the results depends crucially on the quality of the trial wave function. The DMC removes most of the error in the trial wavefunction. DMC is a stochastic projector method that projects out the ground state from the trial wavefunction using an integral form of the imaginary-time Schrödinger equation. For Fermionic systems, the antisymme-

try constraint leads to the Fermion-sign problem that is cured by fixing the nodes of the projected state to be those of an approximate trial wavefunction. The resulting fixed-node error is the main uncontrolled error in DMC. Currently, a systematic improvement of the wavefunction by optimization of an increasing number of variational parameters is the most practical approach for reducing the fixed-node error.^{4,5,6}

Force fields and other approximate methods are sometimes applied to systems that are very different from the systems that were in the fitting database. The question is therefore how reliable are force field based structure predictions of complex structures such as defects, interfaces or clusters. In most studies of such systems only one force field was used but in some exceptionally careful studies, such as in the study of dislocation kinks in silicon⁷ and a comparative study of silicon empirical interatomic potentials⁸, the results of several force fields were compared and significant discrepancies in the results obtained from different force fields were indeed found. To shed light on the accuracy of force fields we examine the configurational density of states obtained by various approximate schemes for silicon. Ideally there would be a one-to-one mapping between stable structures (local minima) obtained using approximate and accurate methods. Consequently the density of configurations per energy interval would be identical for approximate and accurate methods.

II. METHODS

In our study we have included the most common force fields for silicon, namely the Tersoff force field,⁹ the Stillinger-Weber force field,¹⁰ the environmental-dependent interaction potential (EDIP) force field¹¹ and the Lenosky force field. The Tersoff force field, which has infinite range, was smoothly extrapolated to zero by a third order polynomial using cutoff radii that are large enough to ensure a smooth behavior of the potential. The cutoff values were 2.7 and 3.3 Å where the smaller value denotes the radius where the polynomial takes over and the larger value the radius where the polynomial interaction drops to zero. As a representative for tight binding schemes we use the Lenosky tight (LTB) binding scheme.¹² The QMC calculations are performed using the CHAMP code developed by Umrigar, Filippi and Toulouse. The 1s, 2s, and 2p electrons of Si are eliminated using a Hartree-Fock pseudopotential.¹³ The trial wave function consists of a sum of Slater determinants of single-particle orbitals multiplied by a Jastrow factor. The orbitals of the Slater determinant are

taken from a DFT calculation using GAMESS^{14,15} with the B3LYP exchange-correlation functional. The excitations included in the sum of Slater determinants are those with the largest weights in a configuration interaction with single and double excitation (CISD) calculation. Configuration state functions (CSFs), i.e., linear combinations of determinants that have the correct spatial and spin symmetries, are used to reduce the number of variational parameters. The Jastrow correlation function describes electron-electron, electron-nuclear and electron-electron nuclear correlations. The Jastrow parameters and the CSF coefficients are optimized in variational Monte Carlo (VMC) using a recently developed energy minimization method.^{4,5,6} Finally, diffusion Monte Carlo (DMC) calculations using the optimized trial wavefunction and a time step of 0.01 Ha⁻¹ determine the energies of the structures. Most of the calculations employed a single determinant, but to estimate the size of the fixed-node error we performed, for some structures, VMC and DMC calculations with trial wavefunctions containing an increasing number of Slater determinants up to 150. Apart from the preparation of trial wave function for QMC calculations and DFT barrier heights within B3LYP, all other DFT calculations are performed with the BigDFT¹⁶ package, a pseudopotential based^{17,18} DFT code with a wavelet basis set. Wavelets are a systematic basis set and the basis size was chosen sufficiently large that energies were converged to better than to 1 mHa.

III. TRANSITION STATES

According to transition state theory, the height and the shape of saddle points determine the dynamical behavior of a system.¹⁹ Not much effort has been made to assess the effect of approximate energy landscapes on the dynamics of silicon systems. In order to investigate the quality of the silicon potential energy landscape within various schemes we performed simulations to find saddle points of small Si₈ clusters using DFT within the local density approximation. We then compared the barrier heights for these LDA configurations with the heights obtained from other DFT schemes, namely with a generalized gradient approximation functional (PBE), a hybrid functional (B3LYP), and accurate quantum Monte Carlo (QMC) methods. The 8 atom silicon cluster was chosen because for this size, QMC is computationally not too expensive. In agreement with previous work²⁰ we found that the saddle point geometries are nearly identical within different DFT functionals. This justifies the use

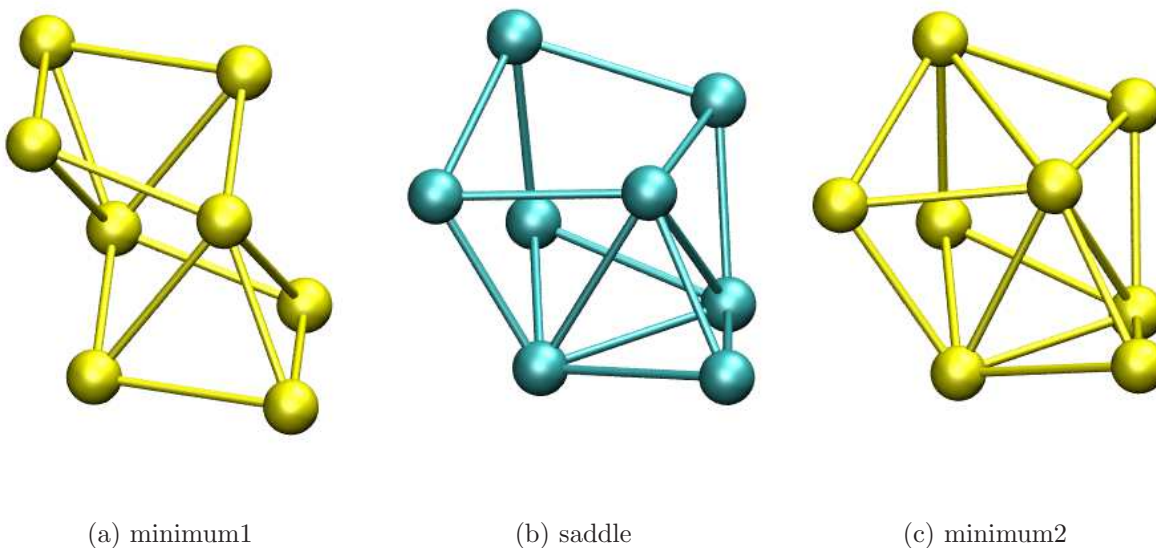
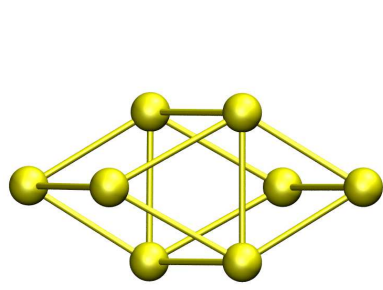


FIG. 1: (color online) The saddle point SP2 (b) and the two neighboring minima (a), (c). It is obvious that the silicon atoms in the saddle point and the minima configurations are all in a similar environment, in particular the saddle point is very similar to the structure (c).

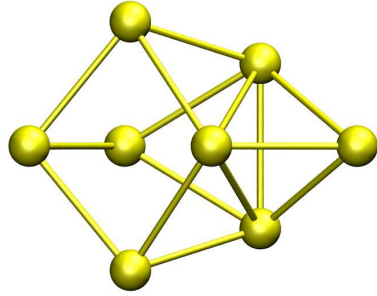
of LDA geometries in all energy calculations. We also compared DFT saddle point results with the Lenosky tight-binding (TB) method. Quantum Monte Carlo has demonstrated its ability to provide accurate reaction barrier heights. Calculated values agreed with the experimental values to within the statistical error bar of 0.07 eV,²¹ for some organic molecules and to within 0.005 eV (see Refs. 22,23) for the well-known exchange reaction $H + H_2 \longrightarrow H_2 + H$. We will therefore consider in the following our QMC results as accurate reference values.

To generate our saddle point configurations, we started with the putative global minimum of the Si_8 cluster²⁴ and using the improved dimer method²⁵ we found six saddle points (SP1 to SP6) which connect the global minimum state to other ones or to itself – the latter corresponds to the exchange of two silicon atoms (SP1 and SP4). Furthermore, two more saddle points (SP7, SP8) are obtained starting from the first low-lying isomer. One of them (SP7) corresponds to the exchange of two atoms. Finding the saddle points and the adjacent minima was done within LDA using the BigDFT¹⁶ package.

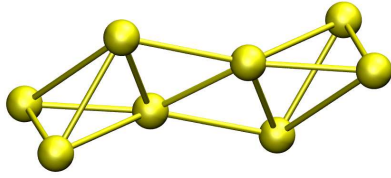
There are numerous publications (for a survey see Ref. 26) in which it is shown that DFT schemes give poor transition state barrier heights for chemical reactions.^{27,28,29} Within LDA and GGA's the results are most unsatisfactory for hydrogen transfer reactions where covalent hydrogen bonds are broken and formed. The most simple and prominent example



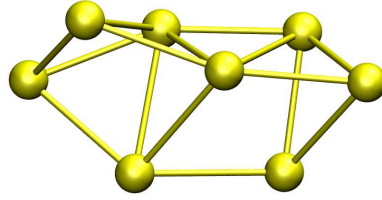
(a) SP1



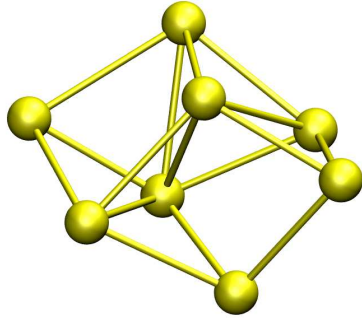
(b) SP2



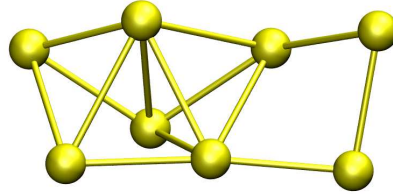
(c) SP3



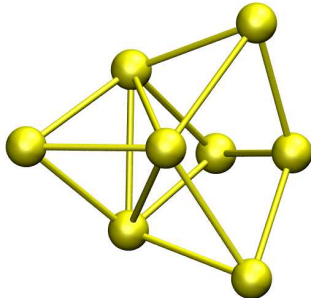
(d) SP4



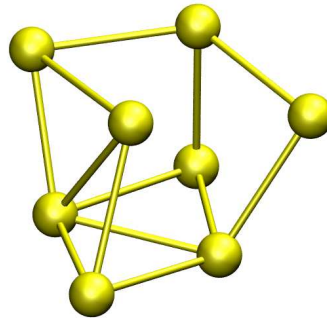
(e) SP5



(f) SP6



(g) SP7



(h) SP8

FIG. 2: (color online) The eight Si_8 saddle points obtained by LDA calculations.

TABLE I: Comparison of the barrier height (BH) energies of eight saddle point (SP) configurations relative to the two neighboring minima calculated with various DFT schemes and QMC. The saddle point and minima configurations are from LDA. The abbreviation for the various DFT functionals are defined in the text. VMC and DMC stand for variational and diffusion QMC, MD-VMC and MD-DMC for multi-determinant VMC and DMC. The HOMO-LUMO gaps for the minima (HLGM) and for the saddle points (HLGS) are calculated within local density approximations using the BigDFT code. The statistical errors are given in parentheses. All energies are in electron volts.

system	HLGM	HLGS	LDA	PBE	B3LYP	VMC	DMC	MD-VMC	MD-DMC	TB
SP1-BH1/2	1.45	0.55	0.359	0.367	0.405	0.434(23)	0.406(13)	0.329(9)	0.338(8)	-0.046
SP2-BH1	1.45	0.41	0.735	0.729	0.770	0.809(20)	0.804(18)			-0.286
SP2-BH2	0.22		0.077	0.094	0.058	0.103(22)	0.069(18)			0.166
SP3-BH1	0.96	0.64	0.043	0.050	0.056	0.046(18)	0.028(15)	0.042(9)	0.028(8)	0.201
SP3-BH2	1.45		2.900	2.689	2.328	2.927(17)	2.845(15)	2.969(8)	2.826(8)	1.934
SP4-BH1/2	1.45	0.13	1.065	1.053	1.075	1.233(18)	1.181(15)	1.131(10)	1.134(7)	0.496
SP5-BH1	1.21	0.42	0.338	0.346	0.324	0.410(18)	0.378(14)			0.398
SP5-BH2	1.45		0.766	0.761	0.800	0.883(17)	0.862(16)			0.019
SP6-BH1	1.49	0.69	0.581	0.573	0.514	0.503(18)	0.536(16)			-0.082
SP6-BH2	1.45		1.198	1.158	1.015	1.283(18)	1.194(16)			0.921
SP7-BH1/2	1.12	0.58	0.289	0.272	0.192	0.228(18)	0.224(16)			0.157
SP8-BH1	0.22	0.82	0.212	0.198	0.041	0.143(17)	0.120(16)			0.144
SP8-BH2	1.12		0.445	0.420	0.406	0.491(18)	0.445(16)			-0.264

is the exchange reaction $H + H_2 \longrightarrow H_2 + H$ where the DFT schemes do not predict a barrier at all. The poor performance seems to be due to poor cancellation of the electrostatic self-interaction errors in the DFT schemes.³⁰ In the literature this problem is known as “self-interaction error” which is related to the delocalization error.³¹ Hybrid functionals, which give a better error cancellation, give improved barrier heights in this case.²⁶ Nevertheless researchers usually resort to wavefunction methods if highly accurate barrier heights are needed for chemical reactions.

Table I shows that in our case the situation is entirely different. Already at the LDA level

the barrier heights are reasonably accurate and actually slightly better than the B3LYP and PBE barriers. How can this surprising accuracy be explained? In contrast to chemical reactions our clusters are never torn apart into fragments when they move along the minimum energy pathway from one local minimum over a saddle point into another local minimum. Even at the transition state (see Figs. 1 and 2) the silicon atoms are all in an environment that is similar to the environment at a local minimum and one cannot distinguish a saddle point configuration from a local minimum energy configuration by inspection. DFT self-interaction errors³¹ are therefore expected to cancel to a large degree.

Since DFT is essentially a one determinant method one would expect that DFT results are particularly poor when transition states have multi-determinant character. This is frequently the case in chemical reactions and under such circumstances multi-reference wavefunction methods have to be employed if accurate barrier heights are needed. Small HOMO-LUMO gaps are an indication of the importance of multi-reference configurations. The HOMO-LUMO gaps of all saddle points and the adjacent minima are presented in Table I. The average HOMO-LUMO gap of saddle points is less than that of the minima by ≈ 0.65 eV. As usual the LDA and GGA gaps are much smaller than the B3LYP gaps which are certainly more accurate. For the configurations with small HOMO-LUMO gaps we also did multi-determinant QMC calculations with as many as 150 determinants. The DMC energies went down by no more than 2 mHa. In Fig. 4, the correlation between the HOMO-LUMO gap and the energy change from single- to multi-determinant calculations is illustrated for seven configurations, in particular for the three configurations that have a HOMO-LUMO gap of less than 0.25 eV. The results show that the influence of a multi determinant wavefunction on the barrier height is very small. Another indication that the multi-determinant character of the saddle point configurations can be neglected is the fact the natural occupation numbers drop rapidly from one to zero. The occupation numbers obtained from CISD calculations using GAMESS with about 70 determinants are shown in Table II.

Table I also shows that the tight binding barrier heights are not reliable. The situation is yet worse for the force fields and we have not even attempted to give error bars. An additional complication, which will be discussed in next section, is that the potential energy surfaces of force fields contain many fake minima and consequently also many fake saddle points connecting the fake minima.

TABLE II: The occupation number of the four highest occupied orbitals and the four lowest unoccupied orbitals of Si_8 clusters obtained from CISD calculations.

system	13th orb.	14th orb.	15th orb.	16th orb.	17th orb.	18th orb.	19th orb.	20th orb.
SP1-min1	1.9814	1.9792	1.9764	1.9716	0.0317	0.0280	0.0253	0.0249
SP1-sadd	1.9804	1.9784	1.9754	1.9711	0.0373	0.0298	0.0280	0.0239
SP2-min2	1.9789	1.9772	1.9741	1.9737	0.0379	0.0286	0.0257	0.0226
SP3-min1	1.9786	1.9773	1.9712	1.9694	0.0351	0.0319	0.0282	0.0272
SP3-sadd	1.9800	1.9763	1.9703	1.9692	0.0385	0.0305	0.0299	0.0267
SP4-sadd	1.9787	1.9769	1.9736	1.9691	0.0396	0.0303	0.0264	0.0217
SP8-min1	1.9789	1.9772	1.9741	1.9737	0.0379	0.0286	0.0257	0.0226

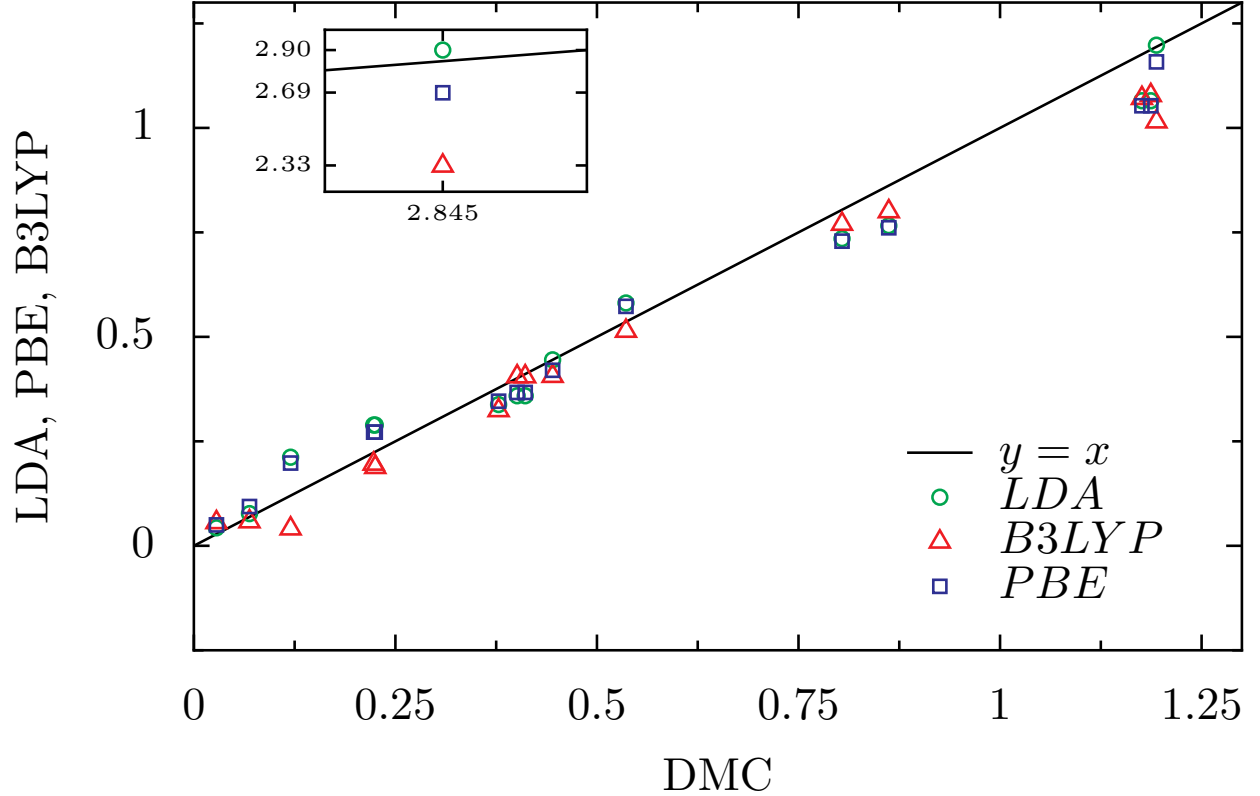


FIG. 3: (color online) The correlation of barrier heights from various DFT functionals with the DMC barrier heights.

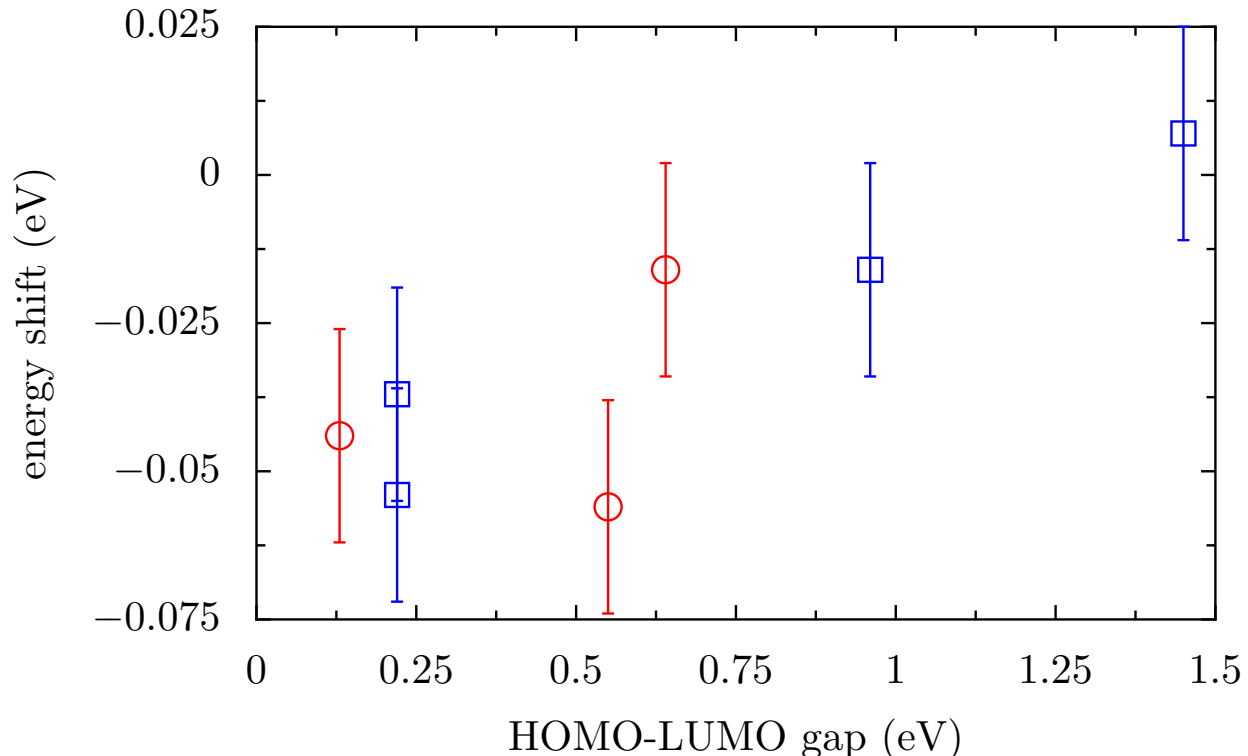


FIG. 4: (color online) The correlation between the energy change from single- to multi-determinant diffusion Monte Carlo calculations with the HOMO-LUMO gap. The (red) circles are for saddle point structures and the (blue) squares are for minimum point structures.

IV. LOW ENERGY CONFIGURATIONS OF SILICON CLUSTERS AND CRYSTALLINE STRUCTURES

A. Funnel-like structure of the PES

The potential energy surface (PES) of the Si_{16} cluster was explored systematically with all of the aforementioned classical many-body potentials and the Tight-Binding scheme using the minima hopping method³² (MHM). The MHM consists of a sequence of consecutive short molecular dynamics runs and geometry relaxations. The MHM is a method that determines the global minimum of a given PES as well as other low-lying energy configurations very efficiently.

Atomic clusters range from structure seekers with well defined ground state configurations which can be found very rapidly with the MHM to glass-like systems for which it is very difficult to find the ground state. The speed with which a system finds its ground state is

evidently a physical property of the system and should carry over to most computational geometry-optimization algorithms.

However, we have found considerable differences in the speed of finding the ground state configuration with the MHM when using the various potentials to describe the Si_{16} cluster. Table III gives the average number n_{MIN} of minima visited before finding the global minimum. The differences in n_{MIN} can be ascribed to the configurational density of states (C-DOS) of the local minima for the particular potentials, discussed in section IV E. A large n_{MIN} indicates a high C-DOS in the low energy region and vice versa. The Si_{16} cluster for instance looks like a structure seeker with the Lenosky force field and more like a glassy system with the Tersoff force field. In agreement with the observation in Fig. 9 the MEAM (Modified Embedded Atom) ansatz³³ of the Lenosky force field gives a relatively smooth potential energy surface.

TABLE III: Average values in 100 MHM runs. n_{MIN} is the number of minima visited before finding the ground state configuration.

Method	n_{MIN}
EDIP	85
Lenosky	10
Reparametrized Lenosky	8
Tersoff	116
Stillinger-Weber	31
Lenosky Tight-Binding	42
DFT	32

B. Ground state and low energy configurations of Si_{16} isomers

A database of stable configurations was generated by visiting 1000 different local minima with the MHM in each potential. To verify the accuracy of the potentials the ten energetically lowest structures were relaxed to the nearest local DFT minimum. The results of the investigation will be discussed separately for each potential and are represented in Fig. 8. The geometrical features to characterize surface properties of Si_{16} isomers are described in

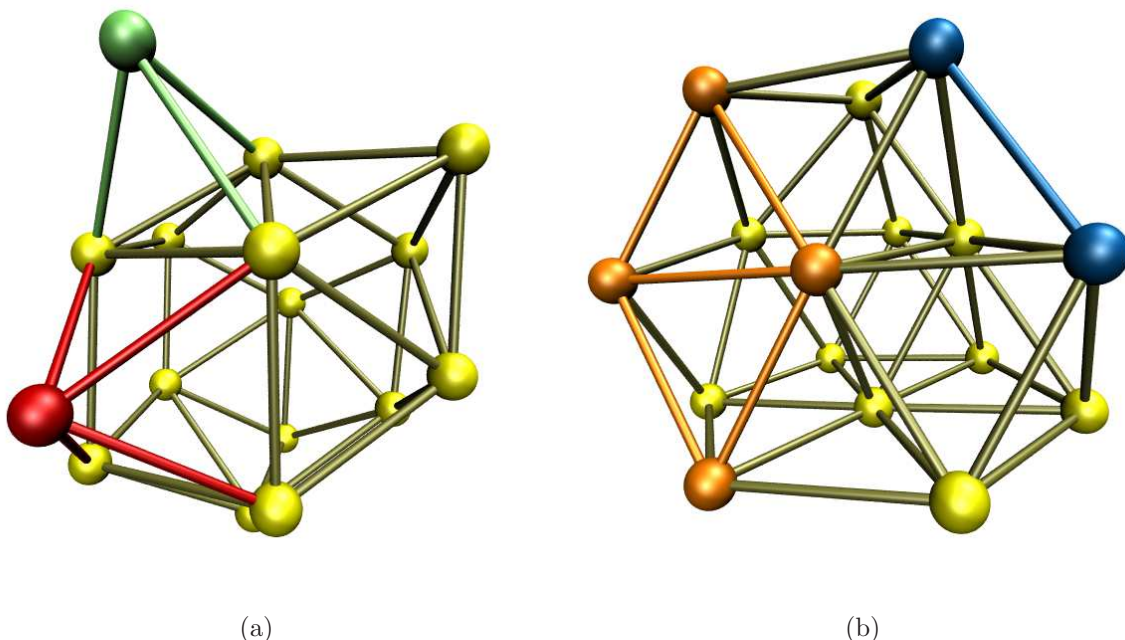


FIG. 5: (color online) (a) A surface atom forms a sharp corner if it defines an acute-angled tetrahedral (green) or pyramidal (red) structure together with its three or four nearest neighbors respectively. (b) Two neighboring surface atoms form a sharp edge if they make an acute-angled tetrahedral structure with the two common nearest neighbors (blue). Four neighboring surface atoms are part of a facet if they form a plane (orange).

Fig. 5.

EDIP: The ground state configuration is a hollow oblate spheroid consisting of four parallel planes. Each plane contains four atoms forming a square which are rotated by 45° with respect to the neighboring planes. The top and bottom squares have an edge length 2.49\AA , the intermediate planes 4.27\AA . In this configuration all atoms are five fold coordinated with an average bond length of 2.50\AA . The first nine excited configurations have the same general features as the ground state and only differ by forming or breaking of up to three bonds. They cover an energy range of 0.5 eV . When relaxed in DFT most of the structures are heavily deformed. In general the void regions within the structure collapse and the shape has a tendency to get elongated. 7 structures show sharp corners and edges and two structures exhibit extended facets. Only one minimum was found to be stable in DFT.

Lenosky: The third and the fourth lowest energy configurations are oblate spheroid

and are the same as the second lowest and the global minimum configurations with EDIP potential respectively. However, the ground state configuration with the Lenosky potential is highly spherical consisting of four hexagonal curved panels with six-fold coordinated center atoms. Although maintaining the general form, the relaxation in DFT reveals that three of the four panels are transformed into planes. Remarkably, an excited configuration was found to relax in DFT to the above mentioned ground state configuration (energy difference in DFT 0.7 eV). Furthermore, there are four spherical and two elongated hollow structures, only one of which is stable with DFT. All other excited states are deformed heavily and the majority show both sharp corners and edges, covering an energy range of 0.4 eV.

Stillinger-Weber: In contrast to the previous two potentials most configurations are highly elongated and often contain pentagonal elements. There are only three exceptions including the ground state configuration which has a hollow elliptical shape formed by 2 square and 8 pentagonal planes. Furthermore, none of the geometries contains over-coordinated atoms. The structures of all minima found with the Stillinger-Weber potential have a strong tendency to contain a large number of sharp corners and only few facets when relaxed in DFT. Although none of the structures are stable in DFT the general elongated form is often conserved and leads to low DFT energies, thus indicating an accurate description of the low energy regions on the PES. The configurational energies are scattered over a range of 0.80 eV.

Tersoff: The ground state geometry of the Tersoff potential is identical to the one found with the Stillinger-Weber potential. Only one of the nine lowest energy configurations other than ground state is elongated, the other eight are very similar to the ground state with hollow spherical shapes. The ninth excited state is 1.4 eV above the ground state. Similar to the Stillinger-Weber potential the structures do not include over-coordinated atoms. All structures are deformed after geometry optimizations with DFT and have a large number of sharp corners.

Lenosky Tight-Binding: The Lenosky Tight-Binding scheme predicts a global minimum configuration which is a slightly distorted Stillinger-Weber and Tersoff ground state geometry. In contrast to the classical potentials both hollow elliptical and elongated structures without void regions are predicted in equal amounts. The energy of the ninth excited state lies only 0.15 eV above the ground state geometry, indicating an overall shallow PES. Although some bond lengths are overestimated, all structures with only one exception were

found to be stable in DFT calculations. However, three configurations with similar geometries converged to the same minimum structure. The ordering of the minima with respect to the energies within the Tight-Binding scheme and the DFT calculations is in fairly good agreement with the ideal correlation (see Fig. 6). While all four classical potentials fail to predict stable low-lying Si_{16} isomers the Lenosky Tight-Binding scheme succeeds in most cases.

C. Flat regions of the PES

During DFT geometry relaxations one can encounter cases where the cluster is distorted considerably even though the energy decreases only slightly. Within these flat regions the norm of the force is small but may increase while the monotonous downhill progress in energy is preserved. Many steps are necessary in the steepest descent DFT geometry relaxation to overcome these flat plateau regions. Only the Lenosky Tight-Binding scheme provides an accurate energy trend when following the DFT relaxation pathway. All classical potentials fail to even describe the lowering of the configurational energy along the pathway (see Fig. 9).

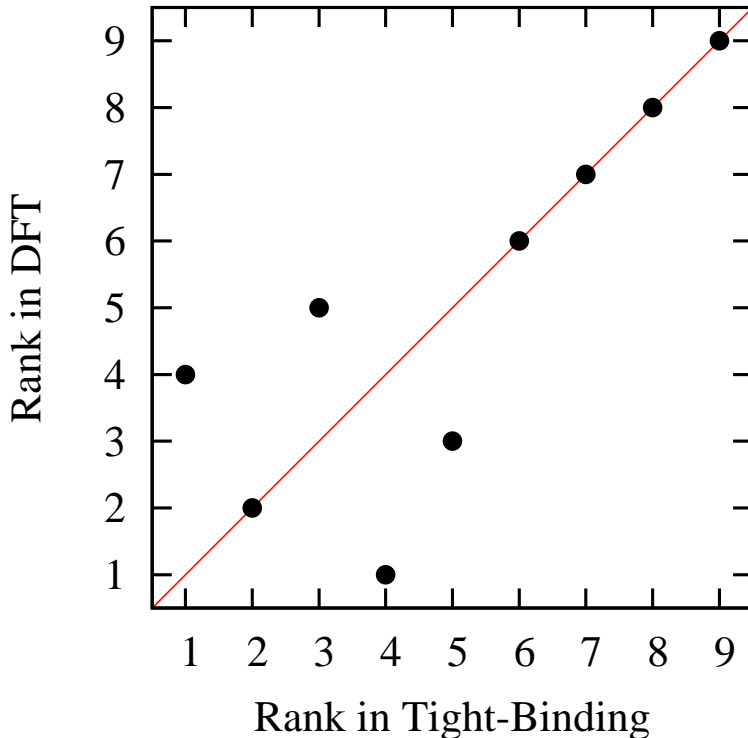
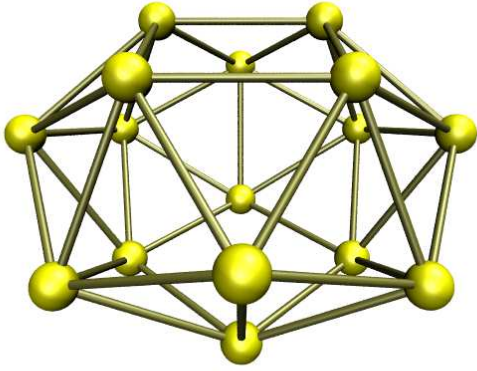
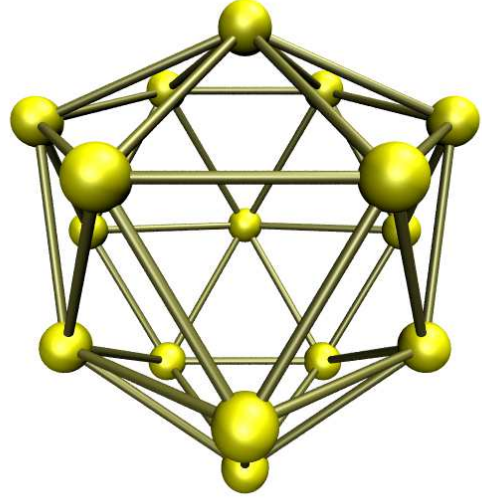


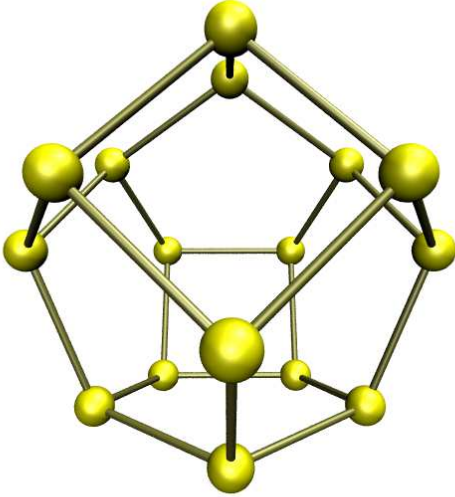
FIG. 6: (color online) Ordering of the local minima energies in Lenosky tight-binding and DFT.



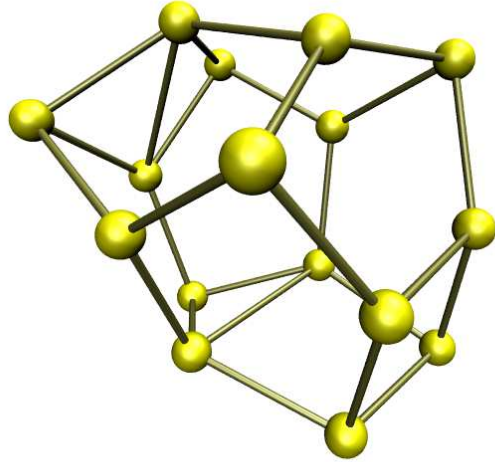
(a)EDIP



(b)Lenosky



(c)Stillinger-Weber/Tersoff



(d)Lenosky Tight-Binding

FIG. 7: (color online) Global minimum configuration of all five potentials found with the minima hopping method.

With the exception of the Lenosky force field these potentials give a strongly oscillating energy surface instead of a flat one along the pathway. This is a first indication that the classical potentials give a too rough PES. The MEAM ansatz of the Lenosky force field seems to give smoother surfaces than the other classical potentials.

TABLE IV: Statistical data related to the Hessian matrix around local minima of up to 120 random configurations (samples) of a Si₃₀ cluster. The second line contains the number of steps used in the geometry relaxation, a combination of preconditioned steepest descent and preconditioned DIIS method (except for the DFT). The corresponding average, minimum and maximum of the largest and smallest eigenvalues of the Hessian matrices are listed in the lines 3 to 8 (in eV/Å²). The last line contains the average condition number κ of the corresponding Hessian matrices. *Values only accurate in the first decimal place.

	EDIP	Lenosky	SW	Tersoff	LTB	DFT*
samples	120	119	120	119	119	40
$\langle \text{steps} \rangle$	111.	99.	131.	39.	126.	
$\langle E_{large} \rangle$	61.	43.	38.	58.	23.	27.
E_{large}^{min}	33.	30.	32.	31.	20.	22.
E_{large}^{max}	116.	95.	44.	137.	27.	30.
$\langle E_{small} \rangle$	0.23	0.44	0.31	0.72	0.18	0.20
E_{small}^{min}	0.004	0.062	0.056	0.15	0.003	0.03
E_{small}^{max}	0.62	1.03	0.78	1.2	0.45	0.61
$\langle \kappa \rangle$	476.	132.	175.	93.	239.	197.

Furthermore, 120 random configurations were relaxed using the different potentials and the largest eigenvalues of the Hessian matrix were calculated when the local minimum configuration was reached. The larger and highly scattered eigenvalues (Table IV) found within the classical potentials indicate that these plateau-like energy landscapes are poorly described by classical force fields. The Stillinger-Weber potential provides the results closest to the Lenosky Tight-Binding scheme, the most accurate among the potentials. This is in agreement with the accurate overall description of low-lying geometries with the Stillinger-Weber potential. The Tersoff potential requires only a small number of relaxation steps, indicating a high number of local minima and the absence of plateau regions on the PES.

TABLE V: The results of ten configurations of each potential relaxed with DFT. The second column shows the number of stable structures. The following columns show the number of structures which relax to the bulk crystal, to a single FFCD or two FFCD which are either neighboring (n-FFCD) or distant (d-FFCD).

Method	Stable	Bulk	FFCD	n-FFCD	d-FFCD
EDIP	2	6	4	0	0
Lenosky	10	1	0	2	7
SW	7	1	4	5	0
Tersoff	2	4	6	0	0
LTB	10	1	1	4	4

D. Defects in crystalline Silicon

The MHM was used to explore the low energy region on the PES of bulk silicon. Starting with crystalline cubic diamond structure consisting of 216 Si atoms, 200000 local minima were found successively for each classical potential during the simulation. For the Lenosky Tight-Binding scheme only 25000 structures could be found due to limited computer time. Periodic boundary conditions with respect to the ground state geometry were used to provide the appropriate bulk conditions. The ten energetically lowest configurations of each potential were used as input configurations for geometry relaxations in DFT.

The correct ground state geometry, the well-known diamond structure, is predicted with all the potentials. However, the structures of the first excited state of different force fields do not coincide. For all potentials except the Lenosky force field it is a single four fold coordinate defect³⁴ (FFCD). The Lenosky potential on the other hand predicts a pair of two four fold coordinated defects³⁴ in different regions of the cell as the lowest energy defect structure. The double FFCD is 3.99 eV higher in energy compared to the diamond structure.

The majority of the eight other low energy geometries in the EDIP potential are structures containing single displaced atoms which are either four or five fold coordinated. Similar structures can be found with the Tersoff potential. All of these excited configurations are unstable in DFT calculations. The Tersoff potential additionally has minima at a variety of slightly distorted FFCDs which are unstable in DFT.

In contrast to the other three force fields, the Lenosky force field always predicts pairs of FFCDs as low-lying energy configurations. They are either neighboring and share a common atom or are distant, i.e., located in different regions of the cell. Even though the single FFCD, which must be the first excited state, is not predicted by the Lenosky force field³⁵, all other low-lying energy configurations from the second to ninth excited states are stable in DFT geometry optimization. Nonetheless, the sequence with respect to the energy does not coincide with the sequence in DFT energies. The Stillinger-Weber force field behaves very similarly. Only three structures were found to be unstable, the other five excited states all contain two interacting FFCDs.

The best accuracy can be found with the Lenosky Tight-Binding scheme. All structures exist on the DFT Born-Oppenheimer surface and the energy sequence is correctly described with the exception of the 9th and 10th excited states. They are exchanged in sequence and show an energy difference of 0.02 eV with the Lenosky Tight-Binding scheme and 0.04 eV when calculated with DFT.

E. Configurational density of states of local minima

To describe the overall characteristics of the potential energy surface we chose the configurational density of states (C-DOS), i.e., the number of configurations per energy interval. We approximate this C-DOS by the minima hopping density of states (MH-DOS) which is obtained simply by sampling the low energy region with the MHM and counting the number of distinct minima found in an energy interval. It has to be stressed that, in the plots we present in this paper, a more or less complete sampling of all minima can only be achieved in a very small interval around the global minimum. Only in this small interval of several eV we observe in the MH-DOS the expected exponential growth of the number of local minima with respect to the energy of the C-DOS. In our plots we show however a much larger energy interval where the number of states is the true number of states multiplied by the probability that a configuration in this energy range will be visited. Since this probability decreases with increasing energy the MH-DOS tends to zero for large energies in all our plots whereas the C-DOS would be orders of magnitude larger. Since the minima hopping method maps out higher and higher energy configurations when the minima hopping run is allowed to continue longer and longer, we can compare the results of our standard

length MHM run, where 200 000 configurations were found, to the results of a longer run, where 1000000 configurations were found. As one can see from Fig. 10 the MH-DOS and C-DOS agree only within the first few bins of the exponential growth region. The lowest energy minima correspond to point defects. The onset of the exponential growth region is due to a growing number of defects (mainly of the FFCD type) which lead continuously to amorphous structures. The longer simulation in Fig. 10 also shows a second peak at around 55 eV. This peak is due to amorphous configurations which are related to a sheared crystalline structure. Since we do not relax the simulation cell sheared structures cannot relax.

The reason why we show the MH-DOS over an energy interval which is much larger than the interval within which we can obtain a reliable C-DOS is the following. If there were good agreement between the C-DOS obtained from different force fields the MH-DOS would also agree. As seen from Fig. 11 the MH-DOS obtained from different force fields are drastically different and one can therefore conclude that the C-DOS are also drastically different. The MH-DOS of all potentials are included in Fig. 11. Stillinger-Weber and the Lenosky Tight-Binding show similar features in the low energy region, e.g., the energy gap between the single FFCD and higher excited states and the spike between 7 and 8 eV. While the EDIP and Tersoff potential show only a single major peak around 10 eV, both Lenosky and Stillinger-Weber have a second peak located at about 35 eV which corresponds, as discussed above, to sheared structures. This is due to the fact that for these two potentials the C-DOS of unsheared amorphous structures is much lower than for the other potentials and the MHM starts therefore sampling higher energy regions corresponding to sheared structures. The differences in the C-DOS are responsible for the different speeds with which the global minimum is found (see Table III).

V. CONCLUSIONS

We have shown that DFT and in particular LDA barrier heights are rather accurate for rearrangement processes occurring in silicon clusters. This is good news since the estimation of diffusion coefficients and other dynamical properties in silicon systems are frequently based on DFT calculations. Since it is well established that DFT schemes give highly accurate results for structural properties, i.e., local minima of the potential energy surface, DFT

calculations are able to provide very reliable potential energy surfaces for silicon systems. The bad news is that force fields, that are widely used for dynamical simulations in large silicon systems, do not faithfully describe the potential energy surface. With the exception of the MEAM based Lenosky force field, all force fields give rise to potential energy surfaces that are too rugged. In an extended crystalline environment most force fields greatly overestimate the configurational density of states because they give rise to many fake defect structures which do not exist in more accurate schemes. The situation is even worse for non-periodic systems where the large majority of stable structures are fake. Simulations based on the use of a single force field should therefore be viewed with caution and should be verified by density functional calculations whenever this is feasible.

VI. ACKNOWLEDGMENTS

We thank Gustavo Scuseria for interesting discussions. Financial support was provided by the Swiss National Science foundations. The calculations were done at the Swiss National Supercomputing center (CSCS) in Manno. The work at Cornell University was supported by the National Science Foundation under grants EAR-0703226 and EAR-0530813. The research used computational resources provided by the National Energy Research Scientific Computing Center, which is supported by the Office of Science of the U.S. Department of Energy, by Teragrid at the National Center for Supercomputing Applications, which is supported by the National Science Foundation and by the Computational Center for Nanotechnology Innovations, which is supported by the state of New York.

An implementation with an identical calling sequence of all the force fields used in this work can be downloaded from www.unibas.ch/comphys/comphys.

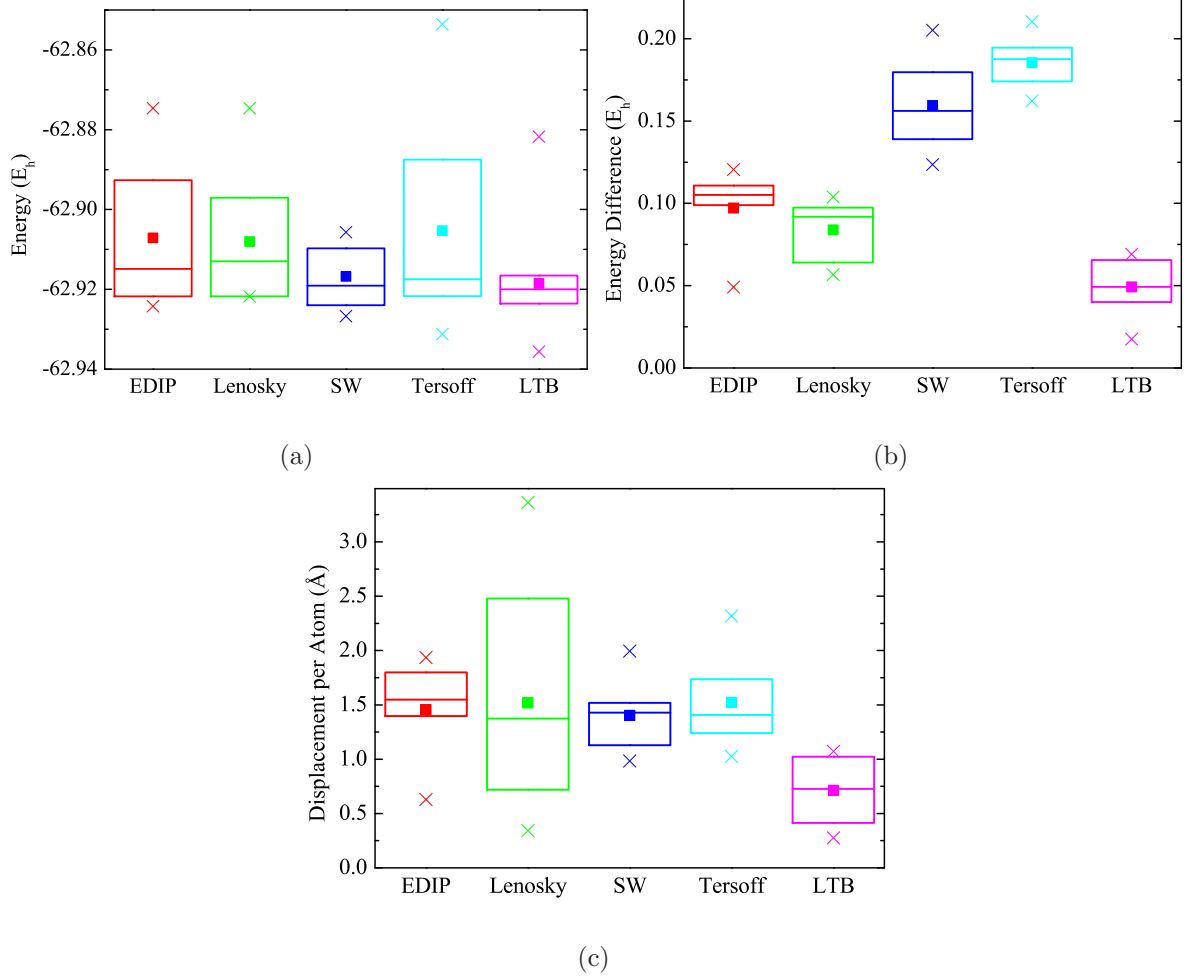


FIG. 8: (color online) The box plots are based on ten low-lying structures of Si_{16} . The boxes contain the values ranging from the lower to the upper quartiles and the median is represented with horizontal lines. The maximum and minimum as well as the mean values are plotted separately with crosses and squares respectively. The absolute energy value found after relaxation in DFT are represented in (a) with arbitrary origin. Plot (b) shows the difference in DFT energy before and after relaxation. Plot (c) shows the average displacements per atom before and after relaxation. Unitary transformations of the initial and final structure were performed to diagonalize the moment of inertia tensor with respect to each atom. The transformations which resulted in the lowest displacement were chosen for the plot. In plots (b) and (c) small values indicate better agreement of the potential with DFT results.

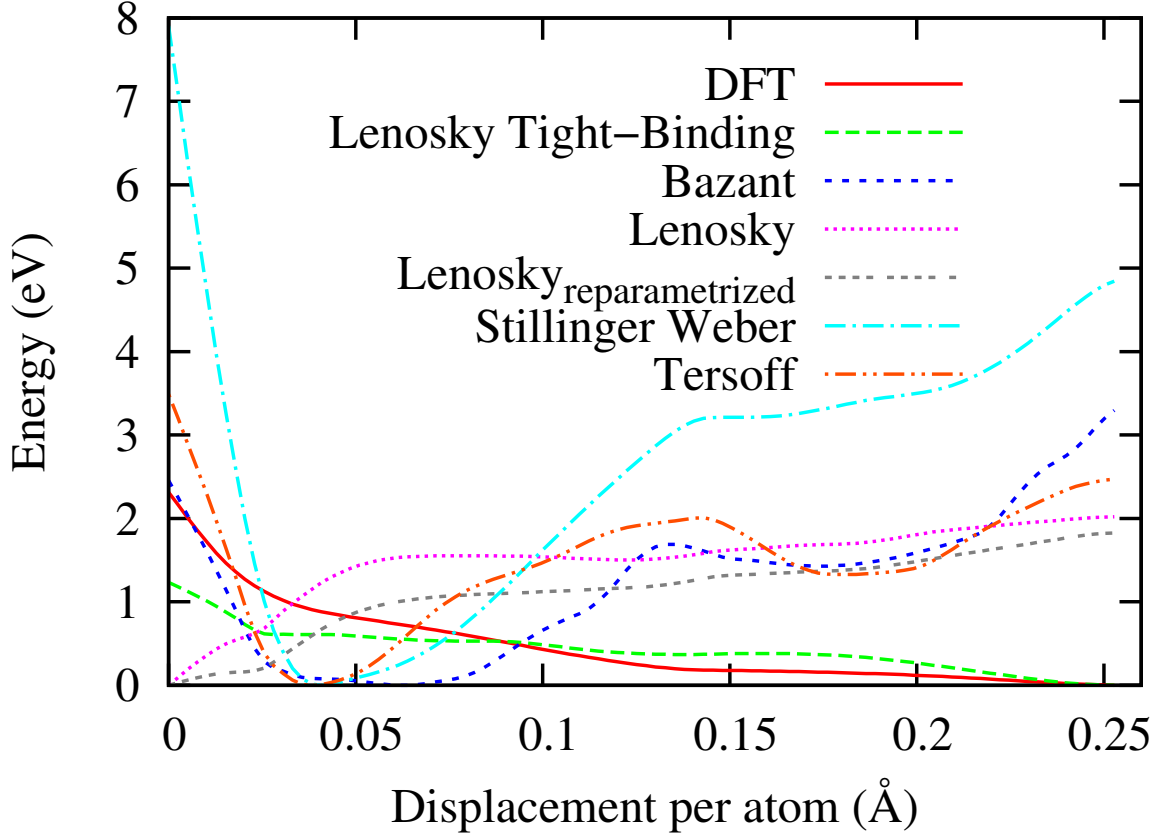


FIG. 9: (color online) Energies of all potentials along a relaxation path in a DFT calculation plotted against the added up norm of the average atomic displacement. The starting configuration is a Lenosky force field local minimum. The energies are shifted such that the minimum values are set to 0. *Lenosky_{reparametrized}* is an unpublished reparametrized Lenosky MEAM in which a single FFCD is stable.

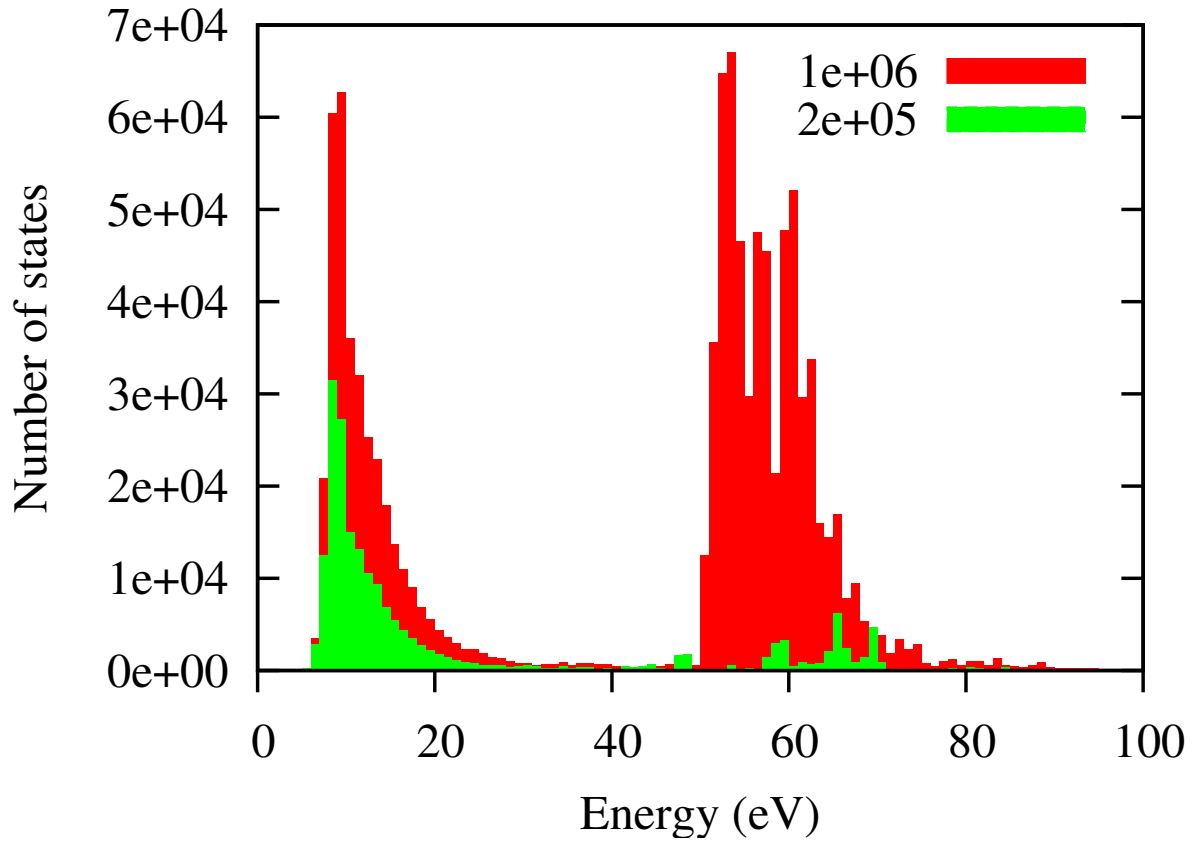


FIG. 10: (color online) The minima-hopping density-of-states, MH-DOS, represented by a histogram with 100 bins. 1×10^6 and 2×10^5 structures were found with the MHM, colored red and green respectively.

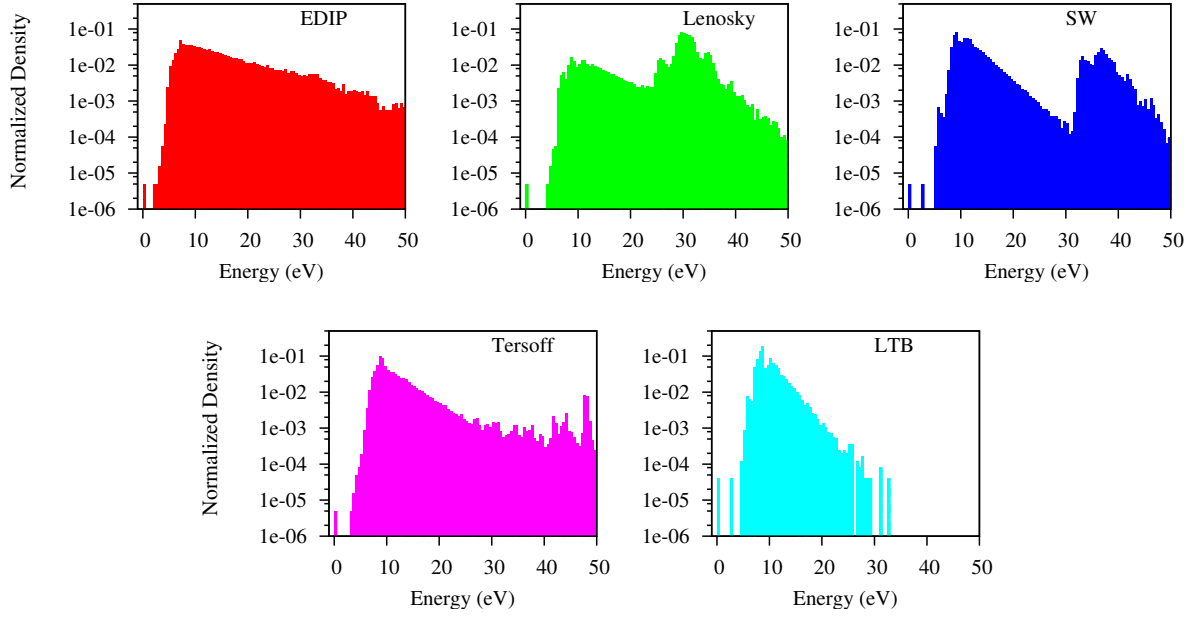


FIG. 11: (color online) The normalized MH-DOS as represented by a histogram consisting of 100 bins on a logarithmic scale. While 200000 values were used for the classical potentials only 25000 could be calculated with the Lenosky Tight-Binding scheme. The energy is shifted such that the ground state has energy 0.

-
- * Stefan.Goedecker@unibas.ch; <http://pages.unibas.ch/comphys/comphys/>
- ¹ F. Valiquette and N. Mousseau, Phys. Rev. B **68**, 125209 (2003).
- ² R. G. Parr and Y. Weitao, *Density-Functional Theory of Atoms and Molecules* (Oxford University Press, USA, 1989).
- ³ J. Perdew, K. Burke, and M. Ernzerhof, Phys. Rev. Lett. **77**, 3865 (1996).
- ⁴ C. J. Umrigar, J. Toulouse, C. Filippi, S. Sorella, and R. G. Hennig, Phys. Rev. Lett. **98**, 110201 (2007).
- ⁵ J. Toulouse and C. J. Umrigar, J. Chem. Phys. **126**, 084102 (2007).
- ⁶ J. Toulouse and C. J. Umrigar, J. Chem. Phys. **128**, 174101 (2008).
- ⁷ A. Pedersen, L. Pizzagalli, and H. Jónsson, J. Phys.: Condens. Matter **21**, 084210 (2009).
- ⁸ H. Balamane, T. Halicioglu, and W. A. Tiller, Phys. Rev. B **46**, 2250 (1992).
- ⁹ J. Tersoff, Phys. Rev. B **39**, 5566 (1989).
- ¹⁰ F. H. Stillinger and T. A. Weber, Phys. Rev. B **31**, 5262 (1985).
- ¹¹ J. ao F. Justo, M. Z. Bazant, E. Kaxiras, V. V. Bulatov, and S. Yip, Phys. Rev. B **58**, 2539 (1998).
- ¹² T. J. Lenosky, J. D. Kress, I. Kwon, A. F. Voter, B. Edwards, D. F. Richards, S. Yang, and J. B. Adams, Phys. Rev. B **55**, 1528 (1997).
- ¹³ D. Alfè, M. J. Gillan, M. D. Towler, and R. J. Needs, Phys. Rev. B **70**, 214102 (2004).
- ¹⁴ M. W. Schmidt, K. K. Baldridge, J. A. Boatz, S. T. Elbert, M. S. Gordon, J. H. Jensen, S. Koseki, N. Matsunaga, K. A. Nguyen, S. Su, et al., J. Comput. Chem. **14**, 1347 (1993).
- ¹⁵ Advances in electronic structure theory: GAMESS a decade later, M.S.Gordon, M.W.Schmidt pp. 1167-1189; in Theory and Applications of Computational Chemistry: the first forty years, C.E.Dykstra, G.Frenking, K.S.Kim, G.E.Scuseria (editors), Elsevier, Amsterdam, 2005.
- ¹⁶ L. Genovese, A. Neelov, S. Goedecker, T. Deutsch, S. A. Ghasemi, O. Zilberberg, A. Bergman, M. Rayson, and R. Schneider, J. Chem. Phys. **129**, 014109 (2008).
- ¹⁷ S. Goedecker, M. Teter, and J. Hutter, Phys. Rev. B **54**, 1703 (1996).
- ¹⁸ C. Hartwigsen, S. Goedecker, and J. Hutter, Phys. Rev. B **58**, 3641 (1998).
- ¹⁹ G. H. Vineyard, J. Phys. Chem. Solids **3**, 121 (1957).
- ²⁰ Y. Kanai, X. Wang, A. Selloni, and R. Car, J. Chem. Phys. **125**, 234104 (2006).

- ²¹ J. C. Grossman and L. Mitas, Phys. Rev. Lett. **79**, 4353 (1997).
- ²² D. M. Ceperley and B. J. Alder, J. Chem. Phys. **81**, 5833 (1984).
- ²³ D. L. Diedrich and J. B. Anderson, Science **258**, 786 (1992).
- ²⁴ W. Hellmann, R. G. Hennig, S. Goedecker, C. J. Umrigar, B. Delley, and T. Lenosky, Phys. Rev. B **75**, 085411 (2007).
- ²⁵ A. Heyden, A. T. Bell, and F. J. Keil, J. Chem. Phys. **123**, 224101 (2005).
- ²⁶ Y. Zhao, N. González-García, and D. G. Truhlar, J. Phys. Chem. A **109**, 2012 (2005).
- ²⁷ S. Andersson and M. Grüning, J. Phys. Chem. A **108**, 7621 (2004).
- ²⁸ M. Grüning, O. V. Gritsenko, and E. J. Baerends, J. Phys. Chem. A **108**, 4459 (2004).
- ²⁹ S. Patchkovskii and T. Ziegler, J. Chem. Phys. **116**, 7806 (2002).
- ³⁰ J. P. Perdew and A. Zunger, Phys. Rev. B **23**, 5048 (1981).
- ³¹ A. J. Cohen, P. Mori-Sánchez, and W. Yang, Science **321**, 792 (2008).
- ³² S. Goedecker, J. Chem. Phys. **120**, 9911 (2004).
- ³³ I. Baskes, Phys. Rev. Lett. **59**, 2666 (1987).
- ³⁴ S. Goedecker, T. Deutsch, and L. Billard, Phys. Rev. Lett. **88**, 235501 (2002).
- ³⁵ An unpublished reparametrized Lenosky MEAM exists in which a single FFCD is stable.